`

SARS-CoV-2 Spike Protein Receptor Binding-ACE2 Interaction Increases Carbohydrate Sulfotransferases and Reduces N-Acetylgalactosamine-4-Sulfatase through Phospho-p38-MAPK and RB-E2F1

Sumit Bhattacharyya, Ph.D.

Joanne K. Tobacman, M.D.*

Jesse Brown VA Medical Center and University of Illinois at Chicago,

Chicago, IL 60612 U.S.A.

Address Correspondence to:
Joanne K. Tobacman, M.D.
820 S. Damen Ave.
Chicago, IL 60612 USA
Telephone 312-569-7826
E-mail: jkt@uic.edu

Abstract

Immunostaining in lungs of patients who died with Covid-19 infection showed increased intensity and distribution of chondroitin sulfate and carbohydrate sulfotransferase (CHST)15 and decline in N-acetylgalactostamine-4-sulfatase (Arylsulfatase B; ARSB). To explain these findings, human small airway epithelial cells were exposed to the SARS-CoV-2 spike protein receptor binding domain (SPRBD) and transcriptional mechanisms investigated. Phospho-p38 MAPK and phospho-Smad3 increased following exposure to the SPRBD, and their inhibition suppressed CHST15 and CHST11 promoter activation. Decline in ARSB was mediated by phospho-38 MAPK-induced N-terminal Rb phosphorylation and the associated decline in E2F1 binding to the ARSB promoter. The increases in chondroitin sulfotransferases were inhibited by the p38-MAPK inhibitor SB203580 and by the Smad3 inhibitor SIS3 and by treatment with the antihistamine desloratadine and the antibiotic monensin. Since accumulation of chondroitin sulfates is associated with fibrotic lung conditions and diffuse alveolar damage, increased attention to p38-MAPK inhibitors may be beneficial in Covid-19 infection.

Introduction

Immunohistochemistry of post-mortem lung tissue from patients with SARS-CoV2 infection showed marked decline in intensity and distribution of N-acetylgalactosamine-4-sulfatase (Arylsulfatase B; ARSB) and increase of total chondroitin sulfate and carbohydrate sulfotransferase (CHST) 15 by immunohistochemistry [1]. The mechanisms leading to these observations were not explained by known signaling pathways known to be activated by exposure to coronaviruses, and this report addresses the underlying reactions leading to these observations in a cell-based model, using normal, human, primary small airway epithelial cells, treated with the SARS-CoV-2 spike protein receptor binding domain protein, based on previous work.

CHST15 [N-acetylgalactosamine 4-sulfate 6-O-Sulfotransferase; B-cell RAG (Recombination Activating Gene)-associated protein; GALNAc4S-6ST] is required for the synthesis of chondroitin sulfate E (CSE) which is composed of alternating β-1,4 and β-1,3 linked D-glucuronate and D-N-acetylgalactosamine-4,6-sulfate residues. Increases in CHST15 or in CSE, have been associated with increased fibrosis in cardiac, lung, and other tissues and with infectivity of dengue virus [2-7], as well as in several malignant cells and tissues, including pancreas, ovary, colon, lung, and brain [8-12]. CHST11 is a carbohydrate sulfotransferase that adds 4-sulfate groups to D-N-acetylgalactosamine residues which are linked to D-glucuronate by β-1,3 glycosidic bonds in chondroitin 4-sulfate or to D-iduronate in dermatan sulfate. Increases in chondroitin 4-sulfate (C4S) and dermatan sulfate follow decline in arylsulfatase B (ARSB, N-acetylgalactosamine-4-sulfatase), since ARSB is the enzyme that removes 4-sulfate groups from N-acetylgalactosamine 4-sulfate residues and is required for the degradation of C4S and dermatan sulfate, as evident by the accumulation of these sulfated glycosaminoglycans in the congenital disease Mucopolysaccharidosis VI (Maroteaux-Lamy Syndrome) caused by mutations of ARSB [13,14]. Accumulation of chondroitin sulfate is recognized as a significant factor in lung fibrosis of different etiologies [15-18], and treatment with recombinant ARSB ameliorated cardiac fibrosis in an animal model [19].

Chondroitin sulfates are vital components of cells and the extracellular matrix (ECM) in all human tissues and throughout living organisms. Biosynthesis of CSE by CHST15 proceeds by transfer of the sulfate residue from 3′-phosphoadenosine-5′-phosphosulfate (PAPS) to the 6-OH of GalNAc4S of C4S [20]. Mechanisms for enhanced CHST15 or CHST11 expression or for decline in ARSB following viral infection have not been reported previously, although the role of sulfated glycosaminoglycans, particularly heparin and heparan sulfate, in SARS-CoV-2 viral uptake and in inhibition of viral infection of human cells has been investigated [21-23].

Many reports have considered how the pathophysiology of Covid-19 relates to interference with the normal balance between effects of Angiotensin (Ang) II and Ang1-7, due to binding of the SARS-CoV-2 spike protein with ACE2 (angiotensin converting enzyme receptor 2). SARS-CoV-2 spike protein binding with ACE2 can inhibit the ACE2-mediated production of Ang1-7 and lead to imbalance between AngII and Ang1-7/Mas receptor effects. AngII causes vasoconstriction initiated by interaction with the AT1 receptor, and decline in opposing vasodilation, due to reduced production of Ang1-7 when ACE2 is bound by the SARS-CoV-2 spike protein, may predispose to unopposed signaling events and significant pathophysiology [24-27]. The impact of inhibition of the renal angiotensin system (RAS) by angiotensin-converting enzyme (ACE) inhibitors or by angiotensin receptor blockers (ARBs) has been considered in relation to treatment and outcome of COVID-19 infection, and studies are ongoing [28-30].

Prior work showed marked increases in expression of CHST15 and CHST11 in rat vascular endothelial cells following exposure to Angiotensin (Ang) II [1]. These increases were largely, but incompletely, inhibited by treatment with an angiotensin receptor blocker, and consistent with possible activation by ACE2. The studies in this report support a sequence of activation of cellular transcriptional events which proceed from direct effects of the interaction between the spike protein receptor binding domain (SPRBD) and the ACE2 receptor in human airway epithelial cells (AEC). Recognition of the usurpation of normal signaling mechanisms by the SARS-CoV-2 spike protein-ACE2 interaction suggests the potential benefit of some targeted

pharmacological interventions based on these pathways. Focus on the specific impact of the spike protein receptor binding domain (SPRBD) interaction with ACE2 on distinct signaling, mechanisms which increase CHST15 and CHST11 expression and inhibit ARSB expression has enabled identification of specific interventions which may have clinical benefit. In the experiments which follow, normal, primary human small airway cells were treated with SPRBD with and without Interferon-β (IFNβ), which augments the expression of ACE2 [31,32], and, thereby, amplifies the impact of the interaction between the SPRBD and ACE2. Elucidation of the roles of phospho-p38MAPK, phospho-Smad3, and Rb phosphorylation provides novel insights into how viral usurpation of endogenous signaling pathways can produce sustained pathophysiological consequences in human cells.

Results

Increases in chondroitin sulfate and carbohydrate sulfotransferase (CHST)15 and decline in N-acetylgalactosamine-4-sulfatase (Arylsulfatase B; ARSB) in post-mortem Covid-19 lung tissue and airway epithelial cells

In post-mortem lung tissue of patients with COVID-19, immunostaining showed decline in intensity and distribution of ARSB, in contrast to increases in total chondroitin sulfate and CHST15 in the alveolar epithelial cells [1]. Representative images from Covid-19 lungs and control tissue of total chondroitin sulfate (**Fig.1a,1b**), ARSB (**Fig.1c,1d**), and CHST15 (**Fig.1e,1f**) are presented. Increased CHST15 was also apparent in vascular smooth muscle cells of the Covid-19 lung tissue, compared to control tissue (**Fig.1g,1h**).

Normal, primary human, small airway epithelial cells (AEC) were treated with the SARS-CoV-19 spike protein receptor binding domain (SPRBD; 2.5 µg/ml x 2h), following exposure to Interferon-β (IFNβ; 10 ng/ml x 24h), which was used to increase the expression of angiotensin converting enzyme 2 (ACE2) receptor, and thereby amplify the effect of SPRBD and better simulate the impact of viral infection**.** The expression of ACE2 increased to more than four times the baseline following IFNβ or the combination of IFNβ and SPRBD, and SPRBD alone did not have any significant impact on ACE2 (**Fig.1i**). Consistent with the observed findings from immunohistochemistry, total chondroitin sulfate and total sulfated glycosaminoglycans (GAGs) increased significantly following exposure to SPRBD and to the combination of SPRBD and IFNβ. Almost two thirds of the increase in the sulfated GAGs was due to the increase by over 5 ug/mg protein of chondroitin sulfate (**Fig.1j**). Sulfotransferase activity increased by over 200% following exposure to the SPRBD and IFNβ (**Fig.1k**). ARSB activity (**Fig.1l**) and mRNA expression (**Fig.1m**) declined following exposure to the SPRBD. The mRNA expression of carbohydrate sulfotransferases CHST15 and CHST11 increased to 3.8 and 2.7 times the control values following exposure to SPRBD and IFNβ ($p<0.001$, $p<0.001$; $n=6$) (**Fig.1n**).

Inhibition of phospho-Thr180/Tyr182-p38-MAPK or of phospho-S423/S425-SMAD3 blocks increases in CHST15 and CHST11

The cultured AEC were treated with inhibitors of cell signaling, including SB203580, an inhibitor of phospho-(Thr180/Tyr182)-p38 MAPK, and NSC23766, a Rho/Rac-1 GTPase inhibitor (**Fig.2a**). Marked declines in expression of CHST15 and CHST11 followed exposure to the phospho-(Thr180/Tyr182)-p38 inhibitor, but NSC23766 had no effect. Increases in CHST15 and CHST11 expression were blocked by SIS3 (specific inhibitor of SMAD3) (**Fig.2b**). Effectiveness of ACE2 silencing was confirmed by QPCR (**Fig.2c**), and the impact of silencing ACE2 tested to confirm that ACE2 was required for the observed effect of the SPRBD. ACE2 siRNA blocked the SPRBD-induced increase in phospho-(Thr180/Tyr182)-p38 (**Fig.2d**), demonstrating dependence on ACE2 for the observed effects. As expected, the increase in phospho-(S423/S425)-SMAD3 following exposure to SPRBD was inhibited by SIS3 (**Fig.2e**), and was also partially inhibited by SB203580 (**Fig.2e**), indicating participation by phospho-p38 in the SPRBD-induced increase in phospho-SMAD3. Phospho-(Thr180/Tyr182)-p38 MAPK was significantly increased following exposure of the cells to SPRBD (**Fig.2f**), but SIS3 had no impact on the increase. Increases in promoter activation of CHST15 (**Fig.2g**) and CHST11 (**Fig.2h**) were abrogated by treatment with either SIS3 or SB203580 following exposure to SPRBD.

Phospho-p38 MAPK mediates decline in ARSB expression through effects on Rb phosphorylation and E2F1

In contrast to the observed increases in CHST11 and CHST15, the mRNA expression and activity of ARSB declined significantly following exposure to the SPRBD (**Fig.1l,1m**). ARSB expression increased following treatment by SB203580 (**Fig.3a**). Neither NSC23766 (**Fig.3a**) nor SIS3 (**Fig.3b**) reversed the effect of SPRBD. ARSB promoter activation was reduced by SPRBD exposure, and treatment with SB203580 reversed the decline in ARSB (**Fig.3c**).

Since phospho-p38-MAPK was reported to activate N-terminal Rb (retinoblastoma protein) phosphorylation [33,34] and thereby inhibit E2F1-DNA binding and the ARSB promoter

has multiple E2F1 binding sites [35], the impact of the p38-MAPK inhibitor SB203580 on Rb phosphorylation following exposure to SPRBD was addressed in the AEC. SB203580 reversed the SPRBD-induced decline in C-terminal phospho-(Ser807/811)-Rb (**Fig.3d**). In contrast, SB203580 reduced the SPRBD-induced increase in N-terminal Rb phosphorylation (phospho - Ser249/Thr252), as shown by Western blot (**Fig.3e**) and corresponding values of phospho-(S249/Thr252)-Rb to total Rb (**Fig.3f**). The phospho-(S249/T252)-Rb to total Rb ratio increased by exposure to SPRBD and declined following SB203580, reflecting the dependence of N-terminal Rb phosphorylation on phospho-p38. Since N-terminal Rb-phosphorylation, in contrast to C-terminal Rb phosphorylation, activates Rb binding with E2F1 [33,34] and reduces availability of E2F for DNA binding, the impact of SPRBD on E2F-DNA binding was assessed. E2F transcription factor-DNA binding assay showed decline following SPRBD-IFNβ exposure and recovery following SB203580 (**Fig.3g**). Chromatin immunoprecipitation (ChIP) assay was performed to assess specific E2F1-binding to the ARSB promoter. Percent DNA input declined following SPRBD-IFNβ exposure, but increased following SB203580 (**Fig.3h**). Agarose gel shows that E2F1-DNA binding to the ARSB promoter was reduced by SPRBD-IFNβ exposure, but was reversed by SB203580 (**Fig.3i**), as confirmed by densitometry (**Fig.3j**). These findings implicate a complex signaling mechanism whereby phospho-p38 MAPK phosphorylates N-terminal Rb, thereby enhancing Rb-E2F1 binding and negatively regulating the ARSB promoter and suppressing ARSB expression.

Effects of Desloratadine, Monensin, and Dexamethasone on expression of CHST15, CHST11, and ARSB

Multiple treatments have been investigated in relation to impact on mortality and morbidity from Covid-19 infection. Both H1 and H2 antihistamine receptor antagonists have been considered, including the H1 antihistamine loratadine and its metabolite desloratadine [36-38]. Treatment of SPRBD-exposed AEC by desloratadine reduced the SPRBD-induced increase of phospho-Thr180/Tyr182-p38-MAPK (**Fig.4a**) and the mRNA expression of CHST15 and CHST11

(**Fig.4b**). Desloratadine also countered the SPRBD-induced decline in ARSB expression (**Fig.4c**) and activity (**Fig.4d**).

The polyether antibiotic monensin, which has been shown to have effects on sulfated glycosaminoglycan biosynthesis [39-41], reduced the SPRBD-induced increases in mRNA expression of CHST15 and CHST11 (**Fig.4e),** but had no effect on the SPRBD-induced decline in ARSB (**Fig.4f**). Dexamethasone, which has been widely used clinically, did not reverse effects of SPRBD on CHST15, CHST11, or ARSB expression.

Discussion

In this report of *in vitro* effects following exposure of cultured normal, human small airway epithelial cells to the SARS-CoV-2 spike protein binding domain, data demonstrate increased expression of chondroitin sulfotransferases CHST15 and CHST11, increased sulfotransferase activity and increased content of chondroitin sulfate, and decline in ARSB expression and activity. Reduced expression of ARSB leads to the accumulation of chondroitin sulfate, since hydrolysis of the 4-sulfate group is required for chondroitin 4-sulfate degradation [42-45]. Both the increases in CHST15 and CHST11 and the decline in ARSB are mediated by phospho-p38 MAPK, and SMAD3 is required for CHST15 and CHST11 expression, whereas the expression of ARSB is regulated by N-terminus Rb phosphorylation and E2F1-Rb interaction, as presented in **Fig.5**. Detailed studies of N-terminal Rb phosphorylation [33,34] present a complex mechanism by which Rb-E2F binding is increased, rather than decreased by C-terminal Rb-phosphorylation. Application of this mechanism of Rb activation by N-terminal phosphorylation, which overrides Rb inhibition by C-terminal phosphorylations, provides a novel, coherent approach to how ARSB expression may be down-regulated following stimulation of phospho-p38 by SPRBD-ACE2 in the AEC.

Study results indicate that pathways leading to decline in ARSB and increases in expression of CHST15 and CHST11 following exposure to the SPRBD require activation of phospho-p38 MAPK. P38-MAPK has been implicated in critical interactions between exogenous exposures, intracellular signaling, and transcriptional events in a wide range of experiments [46-49]. Crosstalk between the p38 and Smad pathways is involved in fibrogenic signaling following AngII and downstream of TGF-β [50-52]. The current experiments provide novel insight into how phospho-p38 participates in the regulation of the biosynthesis and maintenance of 4-sulfated chondroitins.

Other work has shown that when ARSB is inhibited and 4-sulfation sustained, SHP2 binding to chondroitin 4-sulfate is increased, leading to reduced SHP2 activity and sustained

phosphorylation of ERK1,2, JNK, and p38 [14,53-56]. The impact of phospho-38-MAPK on N-terminal Rb phosphorylation, Rb-E2F1 binding, and suppression of ARSB promoter activation, may be part of a loop, in which p38 phosphorylation is sustained, due to enhanced chondroitin 4-sulfate-SHP2 binding which follows decline in ARSB and increased chondroitin 4-sulfation.

Increased understanding of how chondroitin sulfate is involved in the pathogenesis of Covid-19 may help in the development of preventive and therapeutic strategies. The potential benefit of the H1 histamine receptor blocker Desloratadine is suggested by the measured decline in phospho-p38 and by inhibition of the SPRBD effects on expression of CHST15, CHST11 and ARSB, as well as by pharmacological studies that identified desloratadine/loratadine as a mechanism-based target [36-38]. Several clinical studies of H2 blockers on the response in Covid-19 have been reported and additional studies of antihistamines are ongoing [57-59].

Analysis of intensity and distribution of total chondroitin sulfate, CHST15 and ARSB immunohistochemistry in sections from SARS-CoV-2-infected lungs demonstrated marked increase in chondroitin sulfate and prominence of vascular-associated CHST15, in contrast to decline in ARSB [1]. These findings were similar to those observed in diffuse alveolar damage from other causes and suggest that accumulation of chondroitin sulfate might be a significant component in refractory lung disease and pulmonary fibrosis. Previously, decline in ARSB was implicated in the response to hypoxia in human bronchial epithelial cells [60] and in failure of patients with moderate COPD to respond to oxygen therapy [61]. These findings provide additional evidence that decline in ARSB contributes to refractory clinical response in SARS-CoV-2 infection.

By use of the specific spike protein receptor binding domain which binds with ACE2, the experiments in this report have focused on how disruption of normal ACE2 function by the SARS-CoV-2-ACE2 interaction affects signaling in normal human airway cells. In this model, viral uptake does not occur, and other spike protein mediated interactions, such as with TMPRSS2, are not anticipated. A specific p38 isoform, such as p38α, may predominate in the reactions presented

in this report, and future work will help to clarify which p38 isoform(s) is most involved. Also, the precise mechanism by which the SPRBD-ACE2 interaction leads to activation of phospho-p38-MAPK is not yet clarified. Interception of the activation of p38-MAPK emerges as a therapeutic goal, and H1-receptor blockers may directly inhibit phospho-p38 activation and, thereby, prevent the effects of increased expression of CHST15 and CHST11, reduced expression of ARSB, and accumulation of excess chondroitin sulfate following SARS-CoV-2 infection. Also, atypical antibiotics, such an monensin, which directly affect chondroitin 4-sulfate and dermatan sulfate synthesis, may provide new targets to disrupt virus-initiated signaling. Increased attention to the impact of chondroitin sulfates and ARSB in Covid-19 pathobiology and the role of phospho-p38 activation in the mechanisms of their expression may yield new tools and new insights which will reduce the morbidity and mortality of Covid-19.

Materials and Methods

Cell culture and cell treatments

Normal, primary, human small airway epithelial cells (PCS-301-010, ATCC, Manassas, VA) were grown in Airway Epithelial Cell Basal Medium (PCS-300-030, ATCC) supplemented with Bronchial Epithelial Cell Growth Kit (PCS-300-040) and Penicillin-Streptomycin (penicillin 10 U/ml; streptomycin 10 µg/ml), per recommendations. The cells were maintained at 37°C in a humidified 5% CO_2 environment and media were changed every two days. Some cell preparations were treated for 24 hours with Interferon-β (IFNβ; 10 ng/ml; Sigma), a known stimulator of ACE2 (angiotensin converting enzyme 2) expression [31,32]. Following exposure to IFNβ, cells were treated for two hours with purified recombinant SARS-CoV-2 Spike Protein-Receptor Binding Domain protein (SPRBD; AA: Lys310-Leu560; Amsbio, Cambridge, MA; TP750182, 2.5 µg/ml), which was expressed in *E.coli* cells. Some cell preparations were also treated with inhibitors, including: p38 MAPK Inhibitor (SB203580, Adezmapimod, Tocris Bioscience, Bio-Techne, St. Minneapolis, MN; 10µM); Specific Inhibitor of SMAD3 (SIS3, Tocris; 3 µM); and Rho/Rac1 inhibitor (NSC23766, Tocris; 1 ng/ml). The cells were treated with the inhibitors for two hours before exposure to the SPRBD and 22 hours after the start of IFNβ exposure, when used in conjunction with IFNβ. The treatments were continued until cells were harvested at the end of the experiment. Some cell preparations were also treated with Desloratadine (Sigma-Millipore, St. Louis, MO; 32 µM), a histamine H1 receptor antagonist, reported to activate p38-MAPK [36]; the polyether antibiotic Monensin (1 µM; Sigma-Millipore), which inhibits synthesis of dermatan sulfate and chondroitin sulfate [39-41]; or dexamethasone (10 nM or 100 nM; Sigma-Millipore), an accepted treatment of Covid-19 infection for two hours in combination with SPRBD, with or without 24 hours of pretreatment by IFNβ.

Phospho-Thr180/Tyr182-p38 MAPK ELISA

Cell extracts were prepared from both treated and untreated control airway epithelial cells (AEC) in cell lysis buffer (Cell Signaling, Danvers, MA). Phospho-p38 MAPK was measured in

cell samples using a Pathscan® Phospho-p38 MAPK Thr180/Tyr182 Sandwich ELISA (Cell Signaling). Samples were added to the wells of a microtiter plate precoated with a capture antibody to phospho-Thr180/Tyr182-p38 MAPK. The captured phospho-Thr180/Tyr182-p38 MAPK was detected by a p38 MAPK detection antibody. An HRP-linked anti-rabbit antibody was used to recognize the bound detection antibody, and hydrogen peroxide/tetramethylbenzidine (TMB) substrate was used to develop color proportional to the bound HRP. The reaction was stopped, and the optical density of the color was read at 450 nm in a plate reader (FLUOstar, BMG, Cary, NC). The optical densities were normalized by total protein of the cell extract and expressed as percentage of control.

Phospho-(S423/S425)-SMAD3 ELISA

Phosphorylation of SMAD3 in the treated or control nuclear extracts was determined by using a phospho-(S423/S425)-SMAD3 SimpleStep ELISA (Abcam, Waltham, MA), which employs a labeled capture and detector antibody to measure the phospho-SMAD3 in the sample. The entire complex was immobilized in the plate wells by the anti-tag antibody. The bound HRP activity was measured by developing color with hydrogen peroxide/TMB substrate, and the absorbance was measured at 450 nm in a plate reader. The sample values were extrapolated from the standard curve and normalized with total protein in the nuclear extracts.

CHST15, CHST11 and ARSB promoter activity by Luciferase reporter assay

Promoter activity following treatment of the AEC with SPRBD was determined by human CHST15, CHST11 and ARSB promoter constructs in a *Renilla reniformis* luciferase reporter gene (Ren SP; OriGene, Rockville, MD). Transfections were performed with cells at 70% confluence, using FuGENE HD transfection reagent (Promega, Madison, WI). The β-actin promoter (GoClone) construct (SwitchGear Genomics, ActiveMotif, Carlsbad, CA) was used as a positive control, and a scrambled sequence (R01) with the *Renilla* luciferase reporter was a negative control. After 24h incubation, luminescence was read in a microplate reader (BMG). The changes

in luminescence due to modifications in binding to the CHST15, CHST11 or ARSB promoter constructs were detected by the LightSwitch assay system (SwitchGear Genomics).

Arylsulfatase B (ARSB) activity assay

Arylsulfatase B (ARSB) activity measurements were performed using a fluorometric assay, following a standard protocol with 20 µl of homogenate and 80 µl of assay buffer (Na acetate 50mM with barium acetate 20mM, pH 5.6) with 100µl of substrate (5 mM 4-MUS in assay buffer) in a black microplate, as previously detailed [14].

Measurement of total sulfated glycosaminoglycans (sGAG) and chondroitin-4-sulfate

Total sulfated glycosaminoglycans (sGAG) were measured in the cell extracts by sulfated GAG assay (Blyscan™, Biocolor Ltd, Newtownabbey, Northern Ireland) as previously described [62]. This assay detects chondroitin 4-sulfations, chondroitin 6-sulfations, keratan sulfate, heparan sulfate, and heparin, but not hyaluronan or disaccharides. Total chondroitin sulfate (CS) in the samples was determined following immunoprecipitation with a chondroitin sulfate antibody (CS-56, Abcam). Dynabeads (Life Technologies, Carlsbad, CA) were coated with CS-56 antibody, and beads were mixed with samples, incubated, and immunoprecipitated, as previously. Immunoprecipitated CS molecules were eluted and subjected to the Blyscan sulfated GAG assay, as above.

Silencing ACE2 expression

Small interfering (si) RNAs to silence human ACE2 were obtained (Qiagen, Germantown, MD), and their effectiveness determined by quantitative PCR. Cells were grown to ~70% confluency and silenced by adding 0.6 µl of 20 µM siRNA (150 ng), mixed with 100 µl of serum-free medium and 12 µl of HiPerfect Transfection Reagent (Qiagen), as previously [62]. ACE2 expression declined to less than 10% of the control value.

Total sulfotransferase activity

Total sulfotransferase activity was determined using the Universal Sulfotransferase Activity kit (R&D, Minneapolis, MN), as previously. Activities were normalized using total cellular protein and expressed as percentage of control.

Expression of CHST15, CHST11, ARSB, and ACE2

Total RNA was prepared from treated and control cells using an RNeasy Mini Kit (Qiagen). Equal amounts of purified RNAs from the control and treated cells were reverse-transcribed and amplified using Brilliant SYBR Green QRT-PCR Master Mix (Bio-Rad, Hercules, CA). Human β-actin was used as an internal control. QRT-PCR was performed using the following specific primers [63.64]:

CHST11 human (NM_018413) forward: 5′-GTTGGCAGAAGAAGCAGAGG-3′ and reverse: 5′-GACATAGAGGAGGGCAAGGA-3′;

CHST15 human (NM_015892) forward: 5′-ACTGAAGGGAACGAAAACTGG-3′ and reverse: 5′-CCGTAATGGAAAGGTGATGAG-3′;

ARSB (NM_000046) forward: 5′-AGACTTTGGCAGGGGGTAAT-3′ and reverse: 5′-CAGCCAGTCAGAGATGTGGA-3′.

ACE2 (NM_001371415) forward: 5′-CGAAGCCGAAGACCTGTTCTA-3’

and reverse: 5′-GGGCAAGTGTGGACTGTTCC-3′.

Cycle threshold (Ct) was determined during the exponential phase of amplification, as previously [62], and relative expression was expressed compared to control.

Western Blot of phospho-(Ser249/Thr252)-Rb protein

Cell lysates were prepared from control and treated cells in cell lysis buffer (Cell Signaling) with protease and phosphatase inhibitors (Halt Protease and Phosphatase Inhibitor Cocktail, Thermo Scientific, Pittsburgh, PA, USA). Western blots were performed on 10% SDS gels with commercial antibodies to phospho-(Ser249)-Rb protein (Abcam), Rb Protein (Santa Cruz Biotechnology, Santa Cruz, CA), and α-tubulin (Abcam) to probe for the proteins of interest by established procedures. Immunoreactive bands were visualized using enhanced

chemiluminescence (Clarity Western ECL Substrate; Biorad) in Odyssey ® XF Imaging System (LI-COR Biosciences, Lincoln, NE). The optical density of immunoreactive bands was measured, and the optical densities of the phospho-(Ser249)-Rb protein bands were normalized with the optical densities of Rb protein and α-tubulin. The density of treated and control samples was then compared.

Phospho-(Ser807/811)-Rb ELISA

Pathscan® ELISA for phospho-(Ser807/811)-Rb protein was procured (Cell Signaling), and C-terminal phosphorylation of Rb protein was determined in the cell extracts of treated and control AEC according to the protocol. Phospho-(Ser807/811)-Rb protein in the samples was captured by a precoated capture antibody in the wells of the microtiter plate. The captured phospho-(Ser807/811)-Rb protein was further detected by a detection antibody and bound detection antibodies were identified by an HRP-linked secondary antibodies. HRP activity was quantified using hydrogen peroxide/TMB substrate. The enzymatic reaction was stopped by acidic stop solution and color was measured at 450 nm in a plate reader (FLUOstar). The optical densities were normalized by the total protein of the cell extract and expressed as percentage of control.

E2F Transcription Factor (TF) filter plate assay

TF Filter Plate Assay kit and specific DNA probe for E2F were obtained (Signosis, Santa Clara, CA). Nuclear extracts from treated and control cells were mixed with a specific biotin-labeled E2F DNA binding sequence and formed TF-DNA complexes. A filter plate was used to retain the bound DNA probe and remove free probe. The bound pre-labeled DNA probe was then eluted from the filter and collected for quantitative analysis through DNA plate hybridization. The captured DNA probe was further detected with streptavidin-HRP. Luminescence was reported as relative light units (RLUs) by a microplate reader, and the luminescence was normalized by the total protein of the nuclear extract and expressed as percentage of control.

Chromatin Immunoprecipitation (ChIP) of E2F1 and ARSB promoter

ChIP assay was performed utilizing a ChIP assay kit (ActiveMotif, Carlsbad, CA). Control and treated AEC cells were fixed with 1% formaldehyde for 10 min at room temperature, followed by shearing of chromatin by sonication. Sheared DNA was incubated with anti-E2F antibodies (Cell Signaling) for 1 h. Protein–DNA complexes were precipitated by protein A/G-coupled agarose beads. After purification of the DNA from the immunoprecipitated complexes by reversal of cross-linking, followed by proteinase K treatment, real-time RT-PCR was performed using SYBR Green QRT-PCR Master Mix (Bio-Rad). QRT-PCR was performed using the following specific ARSB promoter primers:

Left Primer: 5'-TTAGACCTCTGCCTTTTCACC-3';

Right Primer: 5'-TCCTGTAAAGCCTGCAACAAC-3'.

These primers encompassed the putative E2F1 binding element in the ARSB promoter (SwitchGear Genomics). Band intensity was compared between the treated and the control samples on a 2% agarose gel.

Statistical Analysis

Data presented are the mean ± SD of at least three independent experiments. Statistical significance was determined by one-way analysis of variance followed by post-hoc Tukey's test for multiple determinations using InStat3 software (GraphPad, La Jolla, CA), or by unpaired, two-tailed t-tests, corrected for unequal standard deviations. In the figures, error bars show standard deviations. Statistical significance of differences between controls and experimental samples is presented with exact p-values from t-tests, unless stated otherwise.

Author Contributions: JKT and SB designed the experiments, SB performed the experiments, and wrote the manuscript.

Conflict of Interest: The authors have no conflicts of interest with the content of this article.

References

1. Tzankov A, Bhattacharyya S, Kotlo K, Tobacman JK. Increase in chondroitin sulfate and decline in Arylsulfatase B may contribute to pathophysiology of COVID-19 respiratory failure. Pathobiology. 2022;89(2):81-91.
2. Kai Y, Yoneyama H, Yoshikawa M, Kimura H, Muro S. Chondroitin sulfate in tissue remodeling: Therapeutic implications for pulmonary fibrosis. Respir Investig. 2021; 59(5):576-588.
3. Kai Y, Tomoda K, Yoneyama H, Kitabatake M, Nakamura A, Ito T, et al. Silencing of carbohydrate sulfotransferase 15 hinders murine pulmonary fibrosis development. Mol Ther Nucleic Acids. 2017;6:163–72.
4. Watanabe, K, Arumugam S, Sreedhar R, Thandavarayan RA, Nakamura T, Nakamura M, et al. Small interfering RNA therapy against carbohydrate sulfotransferase 15 inhibits cardiac remodeling in rats with dilated cardiomyopathy. Cell Signal. 2015;27:1517-24.
5. Suzuki K, Arumugam S, Yokoyama J, Kawauchi Y, Honda Y, Sato H, Aoyagi Y, Terai S, Okazaki K, Suzuki Y, Mizumoto S, Sugahara K, Atreya R, Neurath MJ, Watanabe K, Hashiguchi T, Yoneyama H, Asakura H. Pivotal role of carbohydrate sulfotransferase 15 in fibrosis and mucosal healing in mouse colitis. PLoS One. 2016;11(7):e0158967.
6. Sata H, Sagara S, Nakjima N, Akimoto T, Suzuki K, Yoneyama H, Terai S, Yahagi N. Prevention of esophageal stricture after endoscopic submucosal dissection using RNA-based silencing of carbohydrate sulfotransferase 15 in a porcine model. Endoscopy. 2017;49(5):491-497.
7. Kato D, Era S, Watanabe I, Arihara M, Sugiura N, Kimata K, Suzuki Y, Morita K, Hidari KI, Suzuki T. Antiviral activity of chondroitin sulphate E targeting dengue virus envelope protein. Antiviral Res. 2010;88(2):236-243.

8. Ito Z, Takakura K, Suka M, Kanai T, Saito R, Fujioka S, Kajihara M, Yanagisawa H, Misawa T, Akiba T, Koido S, Ohkusa T. Prognostic impact of carbohydrate sulfotransferase 15 in patients with pancreatic ductal adenocarcinoma. Oncol Lett. 2017;13(6):4799-4805.

9. Vallen MJ, Schmidt S, Oosterhof A, Bulten J, Massuger LF, van Kuppevelt TH. Primary ovarian carcinomas and abdominal metastasis contain 4,6-disulfated chondroitin sulfate rich regions, which provide adhesive properties to tumour cells. PLoS One. 2014;9:e111806.

10. Ito Y, Watanabe M, Nishizawa T, Omachi T, Kobayashi T, Kasama S, Habuchi O, Nakayama J. The utility of formalin-fixed and paraffin-embedded tissue blocks for quantitative analysis of N-acetylgalactosamine 4-sulfate 6-O-sulfotransferase mRNA expressed by colorectal cancer cells. Acta Histochem Cytochem. 2007;40(2):53-59.

11. Li F, Ten Dam GB, Murugan S, Yamada S, Hashiguchi T, Mizumoto S, Oguri K, Okayama M, Van Kuppevelt TH, Sugahara K. Involvement of highly sulfated chondroitin sulfate in the metastatsis of the Lewis lung carcinoma cells. J Biol Chem. 2008;283(49):34294-34304.

12. Logun MT, WYnens KE, Simchick G, Zhao W, Mao L, Zhao Q, Mukherjee S, Brat DJ, Karumbaiah L. Surfen-mediated blockade of extratumoral chondroitin sulfate glycosaminoglycans inhibits glioblastoma invasion. FASEB J. 2019;33(11):11973-11992.

13. Harmatz P, Whitley CB, Waber L, Pais R, Steiner R, Plecko B, et al. Enzyme replacement therapy in mucopolysaccharidosis VI (Maroteaux-Lamy syndrome). J Pediatr. 2004; 144(5):574-580.

14. Tobacman JK, Bhattacharyya S. Profound impact of decline in N-acetylgalactosamine-4-sulfatase (arylsulfatase B) on molecular pathophysiology and human diseases. Int J Mol Sci. 2022;29;23(21):13146.

15. Venkatesan N, Ouzzine M, Kolb M, Netter P, Ludwig MS. Increased deposition of chondroitin/dermatan sulfate glycosaminoglycan and upregulation of β1,3-glucuronosyltransferase I in pulmonary fibrosis. Am J Physiol Lung Cell Mol Physiol. 2011; 300:L191-L203.

16. Papakonstantinou E, Klagas I, Roth M, Tamm M, Stolz D. Acute exacerbations of COPD are associated with increased expression of heparan sulfate and chondroitin sulfate in BAL. CHEST 2016;149(3):685-695.

17. Rahmoune H, Lamblin G, Lafitte JJ, Galabert C, Filliat M, Roussel P. Chondroitin sulfate in sputum from patients with cystic fibrosis and chronic bronchitis. Am J Respir Cell Mol Biol. 1991;5(4):315-320.

18. Reeves EP, Bergin DA, Murray MA, McElvaney NG. The involvement of glycosaminoglycans in airway disease associated with cystic fibrosis. ScientificWorldJournal. 2011;11:959-71.

19. Zhao RR, Ackers-Johnson M, Stenzig J, Chen C, Ding T, Zhou Y, Wang P, Ng SL, Li PY, Teo G, Rudd PM, Fawcett JW, Foo RSY. Targeting chondroitin sulfate glycosaminoglycans to treat cardiac fibrosis in pathological remodeling. Circulation. 2018;137(23):2497-2513.

20. Habuchi O, Moroi R, Ohtake S. Enzymatic synthesis of chondroitin sulfate E by N-acetylgalactosamine 4-sulfate 6-O-sulfotransferase purified from squid cartilage. Anal Biochem. 2002;310(2):129-36.

21. Watanabe T, Takeda K, Hiemori K, Minamisawa T, Tateno H. A glycosaminoglycan microarray identifies the binding of SARS-CoV-2 spike protein to chondroitin sulfate E. FEBS Lett. 2021 Sep;595(18):2341-2349.

22. Clausen TM, Sandoval DR, Spliid CB, Pihl J, Perrett HR, Painter CD, et al. SARS-CoV-2 infection depends on cellular heparan sulfate and ACE2. Cell. 2020; 183: 1043–57.

23. Mycroft-West CJ, Su D, Pagani I, Rudd TR, Elli S, Gandhi NS, et al. Heparin inhibits cellular invasion by SARS-CoV-2: Structural dependence of the interaction of the spike S1 receptor-binding domain with heparin. Thromb Haemost. 2020; 120(12): 1700–15.

24. Uhal BD, Li X, Xue A, Gao X, Abdul-Hafez A. Regulation of alveolar epithelial cell survival by the ACE-2/angiotensin 1-7/Mas axis. Am J Physiol Lung Cell Mol Physiol. 2011 Sep;301(3):L269-74.

25. Morales MG, Abrigo J, Meneses C, Simon F, Cisternas F, Rivera JC, Vazquez Y, Cabello-Verrugio C. The Ang-(1-7)/Mas-1 axis attenuates the expression and signalling of TGF-β1 induced by AngII in mouse skeletal muscle. Clin Sci (Lond). 2014;127(4):251-264.

26. Tan HW, Xu YM, Lau ATY. Angiotensin-converting enzyme 2: The old door for new severe acute respiratory syndrome coronavirus 2 infection. Rev Med Virol. 2020;30(5):e2122.

27. Kai H, Kai M. Interactions of coronaviruses with ACE2, angiotensin II, and RAS inhibitors-lessons from available evidence and insights into COVID-19. Hypertens Res. 2020;43(7): 648-654.

28. Williams PB. Renin angiotensin system inhibition as treatment for Covid-19? EClinicalMedicine. 2021;37:101023.

29. Duarte M, Pelorosso F, Nicolosi LN, Salgado MV, Vetulli H, Aquieri A, Azzato F, Castro M, Coyle J, Davolos I, Criado IF, Gregori R, Mastrodonato P, Rubio MC, Sarquis S, Wahlmann F, Rothlin RP. Telmisartan for treatment of Covid-19 patients: An open multicenter randomized clinical trial. EClinicalMedicine. 2021;37:100962.

30. Okoloko O, Vanderwall ER, Rich LM, White MP, Reeves SR, Harrington WE, Barrow KA, Debley JS. Effect of angiotensin-converting-enzyme inhibitor and angiotensin II receptor antagonist treatment on ACE2 expression and SARS-CoV-2 replication in primary airway epithelial cells. Front Pharmacol. 2021;12:765951.

31. Smith JC, Sausville EL, Girish V, Yuan ML, Vasudevan A, John KM, Sheltzer JM. Cigarette smoke exposure and inflammatory signaling increase the expression of the SARS-CoV-2 receptor ACE2 in the respiratory tract. Dev Cell. 2020;53(5):514-529.e3.

32. Klouda T, Hao Y, Kim H, Kim J, Olejnik J, Hume AJ, Ayyappan S, Hong X, Melero-Martin J, Fang Y, Wang Q, Zhou X, Mühlberger E, Jia H, Padera RF Jr, Raby BA, Yuan K. Interferon-alpha or -beta facilitates SARS-CoV-2 pulmonary vascular infection by inducing ACE2. Angiogenesis. 2022;25(2):225-240.

33. Gubern A, Joaquin M, Marquès M, Maseres P, Garcia-Garcia J, Amat R, González-Nuñez D, Oliva B, Real FX, de Nadal E, Posas F. The N-terminal phosphorylation of RB by p38 bypasses its inactivation by CDKs and prevents proliferation in cancer cells. Mol Cell. 2016; 64(1):25-36.
34. Joaquin M, de Nadal E, Posas F. An RB insensitive to CDK regulation. Mol Cell Oncol. 2016;4(1):e1268242.
35. Promo. https://alggen.lsi.upc.es/cgi-bin/promo_v3/promo/promoinit.cgi?dirDB=TF_8.3
36. Noubade R, Milligan G, Zachary JF, Blankenhorn EP, del Rio R, Rincon M, Teuscher C. Histamine receptor H1 is required for TCR-mediated p38 MAPK activation and optimal IFN-gamma production in mice. J Clin Invest. 2007;117(11):3507-18.
37. Oh KK, Adnan M, Cho DH. Network pharmacology study to elucidate the key targets of underlying antihistamines against COVID-19. Curr Issues Mol Biol. 2022;44(4):1597-1609.
38. Mailem RC, Tayo LL. Drug repurposing using gene co-expression and module preservation analysis in acute respiratory distress syndrome (ARDS), systemic inflammatory response syndrome (SIRS), sepsis, and COVID-19. Biology (Basel). 2022;11(12):1827.
39. Hoppe W, Glössl J, Kresse H. Influence of monensin on biosynthesis, processing and secretion of proteodermatan sulfate by skin fibroblasts. Eur J Biochem. 1985 Oct 1;152(1):91-7.
40. Mollenhauer HH, Morré DJ, Rowe LD. Alteration of intracellular traffic by monensin; mechanism, specificity and relationship to toxicity. Biochim Biophys Acta. 1990 May 7;1031(2):225-46.
41. Kajiwara T, Tanzer ML. Undersulfated proteoglycans are induced by the ionophore monensin: study of possible mechanisms. Arch Biochem Biophys. 1982 Mar;214(1):51-5.
42. Silbert JE, Sugumaran G. Biosynthesis of chondroitin/dermatan sulfate. IUBMB Life. 2002; 54(4):177-86.

43. DeSousa JF Jr, Nader HB, Dietrich CP. Sequential degradation of chondroitin sulfate in molluscs. J. Biol. Chem. **1990;** *265:* 20150–20155.

44. Glaser, JH, Conrad HE. Chondroitin SO4 catabolism in chick embryo chondrocytes. *J. Biol. Chem*. **1979**, *254*, 2316–2325.

45. Gorham SD, Cantz M. Arylsulphatase B, an exo-sulphatase for chondroitin 4-sulphate tetrasaccharide*.* Hoppe Seylers Z Physiol. Chem. **1978;***359:*1811–1814.

46. Burton JC, Antoniades W, Okalova J, Roos MM, Grimsey NJ. Atypical p38 signaling, activation, and implications for disease. Int. J. Mol. Sci. 2021;22(8):4183.

47. Martínez-Limón A, Joaquin M, Caballero M, Posas F, de Nadal E. The p38 pathway: From biology to cancer therapy. Int J Mol Sci. 2020 Mar 11;21(6):1913.

48. Grimes JM, Grimes KV. p38 MAPK inhibition: A promising therapeutic approach for COVID-19. J Mol Cell Cardiol. 2020 Jul;144:63-65.

49. Park JK, Fischer R, Dechend R, Shagdarsuren E, Gapeljuk A, Wellner M, Meiners S, Gratze P, Al-Saadi N, Feldt S, Fiebeler A, Madwed JB, Schirdewan A, Haller H, Luft FC, Muller DN. p38 mitogen-activated protein kinase inhibition ameliorates angiotensin II-induced target organ damage. Hypertension. 2007 Mar;49(3):481-9.

50. Li SN, Zhang JR, Zhou L, Xi H, Li CY, Zhao L. Sacubitril/Valsartan decreases atrial fibrillation susceptibility by inhibiting angiotensin II-induced atrial fibrosis through p-Smad2/3, p-JNK, and p-p38 Signaling Pathways. J Cardiovasc Transl Res. 2022; 15(1):131-142.

51. Javelaud D, Mauviel A. Crosstalk mechanisms between the mitogen-activated protein kinase pathways and Smad signaling downstream of TGF-beta: implications for carcinogenesis. Oncogene. 2005;24(37):5742-50.

52. Furukawa F, Matsuzaki K, Mori S, Tahashi Y, Yoshida K, Sugano Y, Yamagata H, Matsushita M, Seki T, Inagaki Y, Nishizawa M, Fujisawa J, Inoue K. p38 MAPK mediates fibrogenic signal through Smad3 phosphorylation in rat myofibroblasts. Hepatology. 2003;38(4):879-89.

53. Bhattacharyya S, Feferman L, Tobacman JK. Inhibition of phosphatase activity follows decline in sulfatase activity and leads to transcriptional effects through sustained phosphorylation of transcription factor MITF. PLoS One. 2016 Apr 14;11(4):e0153463.

54. Bhattacharyya, S.; Feferman, L.; Han, X.; Ouyang, Y.; Zhang, F.; Linhardt, R.J.; Tobacman, J.K. Decline in arylsulfatase B expression increases EGFR expression by inhibiting the protein-tyrosine phosphatase SHP2 and activating JNK in prostate cells. *J.Biol. Chem*. **2018,** *293*, 11076–11087.

55. Bhattacharyya S, Feferman L, Terai K, Dudek AZ, Tobacman JK. Decline in arylsulfatase B leads to increased invasiveness of melanoma cells. Oncotarget. 2017 Jan 17;8(3):4169-4180.

56. Bhattacharyya S., Feferman, L.; Tobacman, J.K. Chondroitin sulfatases differentially regulate Wnt signaling in prostate stem cells through effects on SHP2, phospho-ERK1/2, and Dickkopf Wnt signaling pathway inhibitor (DKK3). *Oncotarget* **2017**, *8*,100242–100260.

57. Cheema HA, Shafiee A, Athar MMT, Shahid A, Awan RU, Afifi AM, Shah J, Jalal PK. No evidence of clinical efficacy of famotidine for the treatment of COVID-19: a systematic review and meta-analysis. J Infect. 2022;1:S0163-4453(22)00683-1.

58. Mohseni M, Raissi V, Sharifan Y, Barikro K, Amiri S, Mohseni MS, Raeisi F, Masoumi K, Khodakarami S, Raiesi O. Therapeutic status of famotidine in COVID-19 patients: A review. Infect Disord Drug Targets. 2022;22(3):e070122200096.

59. Brennan CM, Nadella S, Zhao X, Dima RJ, Jordan-Martin N, Demestichas BR, Kleeman SO, Ferrer M, von Gablenz EC, Mourikis N, Rubin ME, Adnani H, Lee H, Ha T, Prum S, Schleicher CB, Fox SS, Ryan MG, Pili C, Goldberg G, Crawford JM, Goodwin S, Zhang X, Preall JB, Costa ASH, Conigliaro J, Masci JR, Yang J, Tuveson DA, Tracey KJ, Janowitz T. Oral famotidine versus placebo in non-hospitalised patients with COVID-19: a randomised, double-blind, data-intense, phase 2 clinical trial. Gut. 2022;71(5):879-888.

60. Bhattacharyya S, Tobacman, JK. Hypoxia reduces arylsulfatase B activity and silencing arylsulfatase B replicates and mediates the effects of hypoxia. PLoS One. 2012;7(3):e33250.

61. Seo, M.; Qiu, W.; Bailey, W.; Criner, G.J.; Dransfield, M.T.; Fuhlbrigge, A.L.; Reilly, J.J.; Scholand, M.B.; Castaldi, P.; Chase, R.; et al. Genomics and response to long-term oxygen therapy in chronic obstructive pulmonary disease. *J. Mol. Med.* **2018**, *96*, 1375–1385.
62. Bhattacharyya S, Feferman L, Tobacman JK. Arylsulfatase B regulates versican expression by galectin-3 and AP-1 mediated transcriptional effects. Oncogene. 2014;33(47):5467-5476.
63. Untergasser A, Cutcutache I, Koressaar T, Ye J, Faircloth BC, Remm M, et al. Primer3 - new capabilities and interfaces. Nucleic Acids Res. 2012;40(15):e115.
64. Koressaar T, Remm M. Enhancements and modifications of primer design program Primer3. Bioinformatics. 2007;23(10):1289-1291.

Figure Legends

Fig. 1. Chondroitin sulfate, Arylsulfatase B, and CHST15 in Covid-19 and normal control lung tissue and in human small airway epithelial cells.

a,b. In lung tissue obtained post-mortem from patients who died due to SARS-CoV-2 infection, immunohistochemistry showed increased total chondroitin sulfate compared to normal control lung tissue. **c,d.** In contrast, intensity and distribution of ARSB were markedly reduced in the Covid-19 lung tissue. Marked decline is evident in the membrane immunostaining, compared to the normal control. **e,f.** Carbohydrate sulfotransferase (CHST) 15 which is the sulfotransferase that adds a 6-sulfate group to chondroitin 4-sulfate to form chondroitin-4,6-sulfate (chondroitin sulfate E), has regions of marked intensity of immunostaining in both the Covid-19 lung and the normal lung. **g,h.** In vascular smooth muscle tissue of the Covid-19 lung, the CHST15 immunostaining is much more intense and less diffuse than in the normal lung vascular tissue. **i**. Treatment of the cultured cells with Interferon (IFN)β amplifies the impact of SPRBD by increasing the expression of ACE2 more than four times the control level ($p<0.1x10^{-5}$, n=6). **j.** Corresponding to the findings in the infected lung tissue, total chondroitin sulfate (CS) increased by ~2 ug/g protein (p=0.001, n=6) and total sulfated glycosaminoglycans increased by over 3 ug/g protein (sGAG) (p=0.0005, n=6) in the AEC following exposure to the SPRBD. Increases are more following combined treatment with SPRBD and IFNβ (>5 µg/g protein for CS, n=6; 7.7 µg/g protein for sGAG, n=6). **k.** Consistent with the observed increases in chondroitin sulfate in Covid-19 lung tissue and in the airway cells, sulfotransferase activity increased by 63% following SPRBD and by over 200% following the combination of SPRBD and IFNβ (n=6, n=6) **l.** Arylsulfatase B (ARSB) activity declined in the AEC following exposure to the SPRBD (p=0.005, n=6), and declined over 50% by the combined exposure to SPRBD and IFNβ. **m**. The mRNA expression of ARSB also declined ($p=2.6x10^{-5}$; n=6) following SPRBD, and declined further following exposure to the combination of SPRBD and IFNβ. **n.** Expression of both CHST15 and of CHST11, which transfers

4-sulfate groups to N-acetylgalactosamine residues to create chondroitin 4-sulfate, is significantly upregulated following exposure to the SPRBD and the combination of SPRBD and IFNβ.

All of the p-values were determined using unpaired t-test, two-tailed, with unequal variance, and error bars represent one standard deviation.

[ACE2=angiotensin converting enzyme 2 receptor; AEC=normal, human small airway epithelial cells; ARSB=arylsulfatase B=N-acetylgalactosamine-4-sulfatase; SPRBD=SARS CoV-2 spike protein receptor binding domain]

Fig.2. SMAD3 and p38-MAPK inhibitors abrogate the effects of SPRBD.

a. The SPRBD- and SPRBD+IFNβ- induced increases in the mRNA expression of CHST15 and CHST11 were significantly reduced following exposure to SB203580, the p38-MAPK inhibitor. In contrast, NSC23766, a Rho/Rac-1 GTPase inhibitor, had no impact on their expression. **b**. SIS3, an inhibitor of phospho-Smad3, inhibited the SPRBD- and SPRBD+IFNβ- induced increases in expression of CHST15 and CHST11. **c.** Expression of ACE2 was inhibited by ACE2 specific siRNA following exposure to SPRBD alone or with IFNβ. **d.** Following silencing of ACE2 by siRNA, the SPRBD- and SPRBD+IFNβ- induced increases in phospho-T180/T182-p38 MAPK were inhibited. **e**. The SPRBD- and SPRBD+IFNβ- induced increases in phospho-S423/S425 SMAD3 were completely inhibited by SIS3 and, to a lesser extent, by SB203580, the p38 MAPK inhibitor**.** **f.** The SPRBD and SPRBD+IFNβ- induced increases in phospho-Thr180/Tyr182-p38 were unaffected by exposure to SIS3 and were inhibited by SB203580. **g,h.** Promoter activity of CHST15 and CHST11 was enhanced by exposure to SPRBD and to a greater extent by the combination of IFNβ and SPRBD. Both SIS3 and SB203580 inhibited promoter activation.

[SIS3=specific inhibitor of SMAD3]. All p-values were determined by unpaired t-test, two-tailed, with unequal variance, and with at least three independent experiments. Error bars represent one standard deviation.

Fig.3. Exposure to spike protein receptor binding domain inhibits ARSB expression by activation of phospho-p38 MAPK and phospho-(S249/T252)-RB-E2F1 interaction.

a. ARSB mRNA expression was unaffected by NSC23766, but following exposure to the p38-MAPK inhibitor SB203580, mRNA expression was restored to baseline control values. **b.** In contrast, SIS3 had no impact on the SPRBD- or SPRBD+IFNβ- induced decline in ARSB expression. **c.** ARSB promoter activation was reduced by SPRBD and by SPRBD+IFNβ. These declines were reversed by exposure to SB203580, but not by SIS3. **d.** Following treatment with SPRBD or SPRBD+IFNβ, C-terminal phospho-(Ser807/811)-Rb declined as shown by ELISA. These declines were reversed by SB203580, but not by SIS3. **e.** In contrast to the decline in C-terminal Rb phosphorylation, exposure to SPRBD+IFNβ increased N-terminus phospho-(S249)-Rb, as detected by Western blot. This increase was inhibited by SB203580, and total Rb was unchanged. **f.** Densitometry confirms the impression of Western blot and shows the ratio of phospho-S249-Rb to total Rb following SPRBD+IFNβ has increased to 3.89 times the baseline. **g**. Following exposure to SPRBD and SPRBD+IFNβ, E2F-DNA binding declined significantly, and SB203580 reversed the declines. **h.** %DNA input declined following SPRBD+IFNβ and increased following inhibition of p38-MAPK by SB203580. **i.** Chromatin immunoprecipitation (ChIP) shows decline in E2F1 binding to the ARSB promoter following exposure to SPRBD+IFNβ; decline was reversed by SB203580. Agarose gel demonstrates no effect of the IgG negative control on E2F1 binding to the ARSB promoter at baseline, IFNβ control, reduced binding following SPRBD+IFNβ, and reversal of the decline following treatment with SB203580. **j**. Measurements of optical density confirm the impression from the gel.

P-values were determined by unpaired t-tests, two-tailed with unequal variance, with n of at least 3 independent experiments. Error bars show one standard deviation.

Fig. 4. Effects of selected agents on expression of CHST15, CHST11, and ARSB.

A. The antihistamine desloratadine reduced by 62% the SPRBD-induced increase in T180/T182 phospho-p38-MAPK in the AEC. **B.** Consistent with the decline in phospho-p38, desloratadine reduced the SPRBD-induced and SPRBD with IFNβ-induced increases in CHST15 (p=0.045, p=0.0041 with IFNβ) and CHST11 expression (p=0.008, p=0.0017 with IFNβ, unpaired t-tests,

two-tailed, unequal variance, n=3)**. C, D**. Consistent with the observed decline in ARSB, desloratadine partially reversed the SPRBD-induced decline in ARSB activity (from 64.7 to 73.4 nmol/mg protein/h and from 41.0 to 61.8 nmol/mg protein/h with IFNβ; n=3) and expression (0.71 to 0.87 and 0.46 to 0.74 with IFNβ, fold-change compared to control; n=3). **E.** The polyether antibiotic monensin, which modifies dermatan sulfate biosynthesis and processing [39-41], reduced the SPRBD-induced increases in CHST15 mRNA (p=0.003, p=0.006 with IFNβ) and CHST11 (p=0.003, p=0.002 with IFNβ; fold-change compared to control, unpaired t-tests, two-tailed, unequal variance). **F**. Monensin had no significant impact on the SPRBD-induced decline in ARSB.

Fig. 5. SARS-CoV-2 spike protein binding with ACE2 initiates transcriptional events which modify chondroitin sulfation through activation of phospho-p38 MAPK.

Schematic of SARS-CoV-2 spike protein binding domain (SPRBD) peptide interaction and initiation of transcriptional events which modify chondroitin sulfation through activation of phospho-p38 MAPK. Both p38 MAPK and phsopho-Smad3 lead to increased expression of CHST15 and CHST11. AngII interaction with AT1 is also expected to increase phospho-p38. Phospho-p38 leads to N-terminal phosphorylation and activation of Rb with enhanced binding of E2F1, which reduces ARSB promoter activation due to reduced binding of E2F1. [ACE2=angiotensin converting enzyme 2; AngII=angiotensin II; ARSB=arylsulfatase B; AT1R=angiotensin II receptor type 1; AT2R=angiotensin II receptor type 2; CHST=carbohydrate sulfotransferase; pRb=retinoblastoma protein; SMAD=Suppressor of Mothers against Decapentaplegic; SPRBD=SARS-CoV-2 spike protein receptor binding domain]

Fig. 1. Chondroitin sulfate, Arylsulfatase B, and CHST15 in Covid-19 and normal control lung tissue and in human small airway epithelial cells.

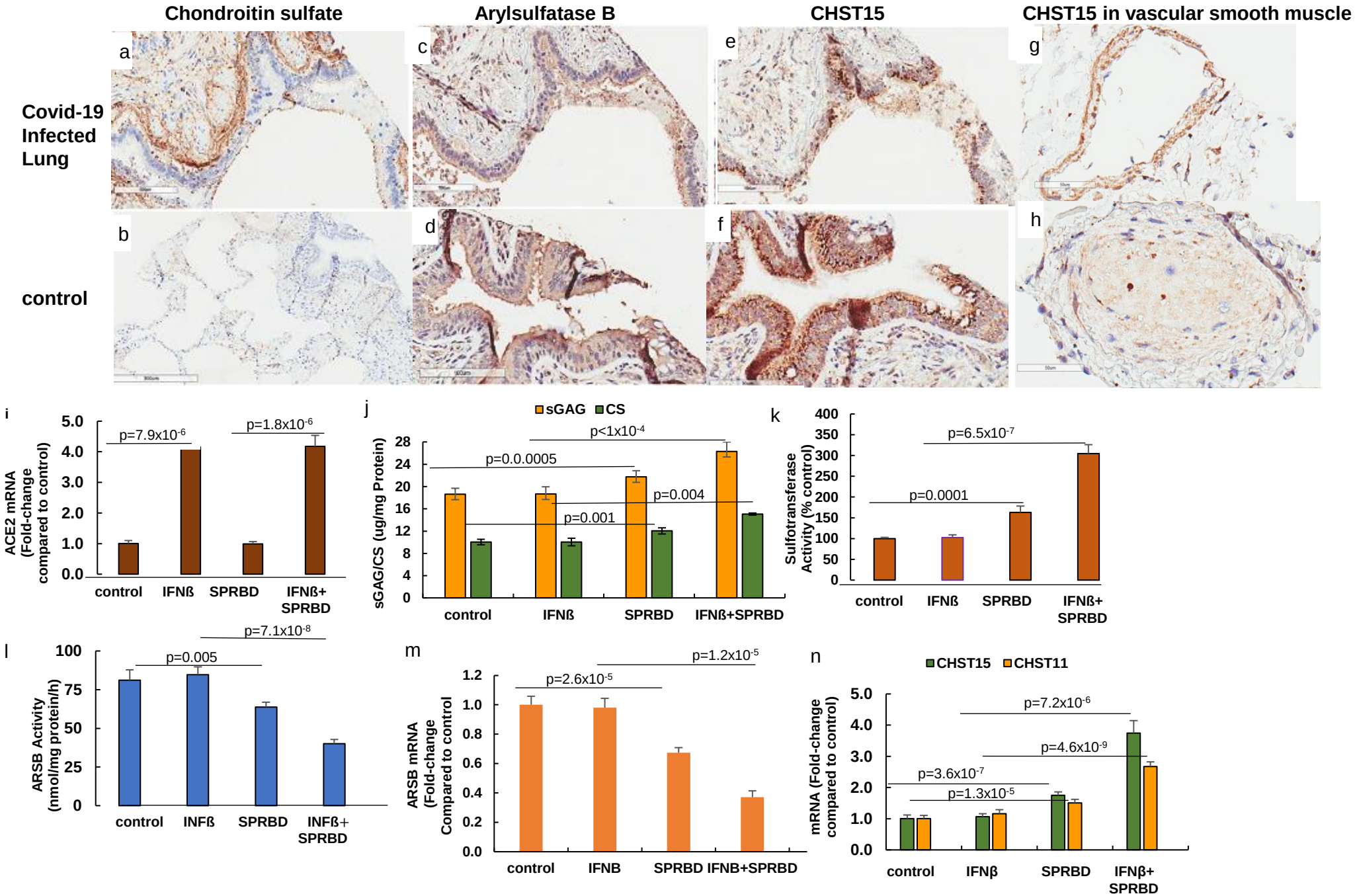

Fig.2. SMAD3 and p38-MAPK inhibitors abrogate the effects of SPRBD.

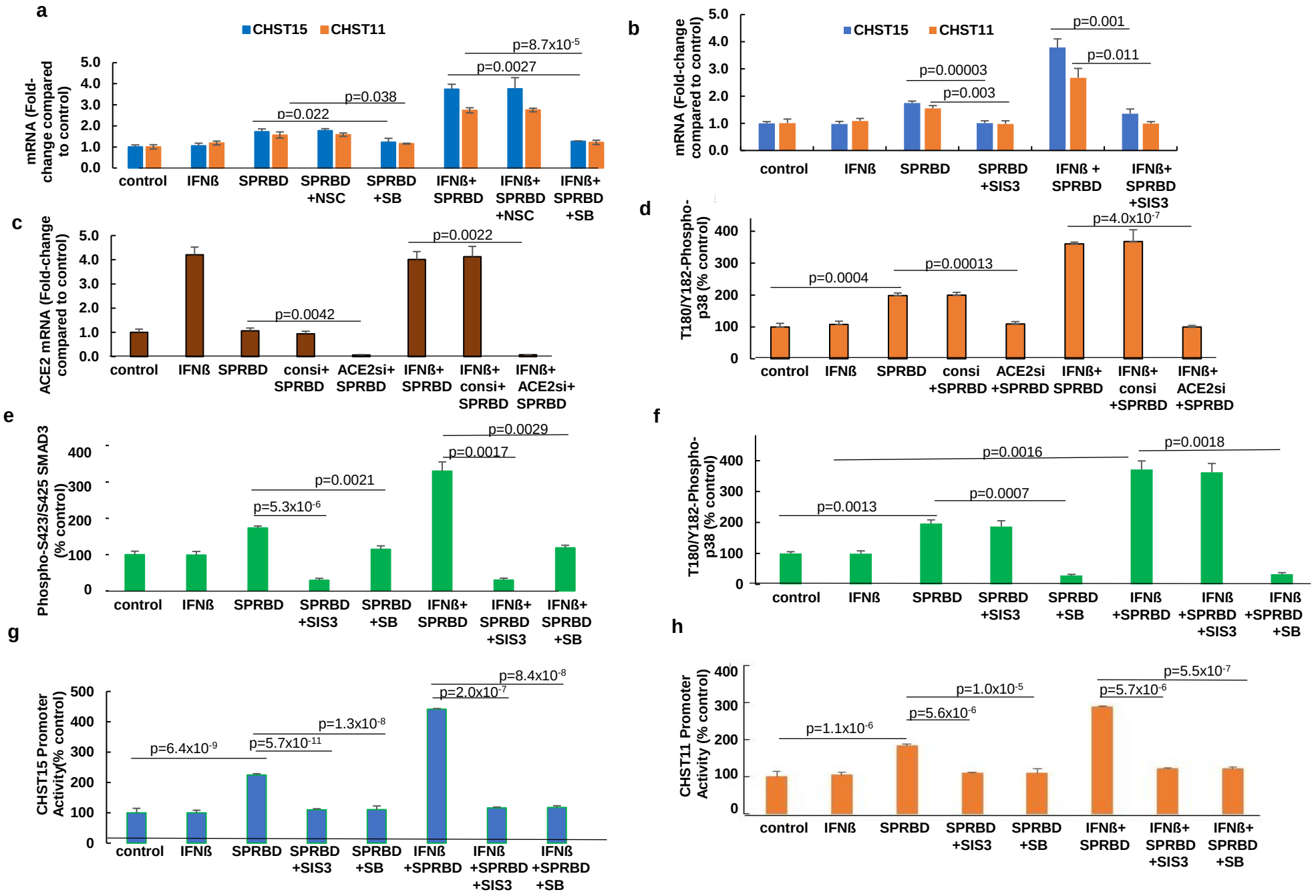

Fig.3. Spike protein receptor binding domain Inhibits ARSB activity and expression by activation of phospho-p38 MAPK and phospho-(S249/T252)-RB-E2F1 interaction.

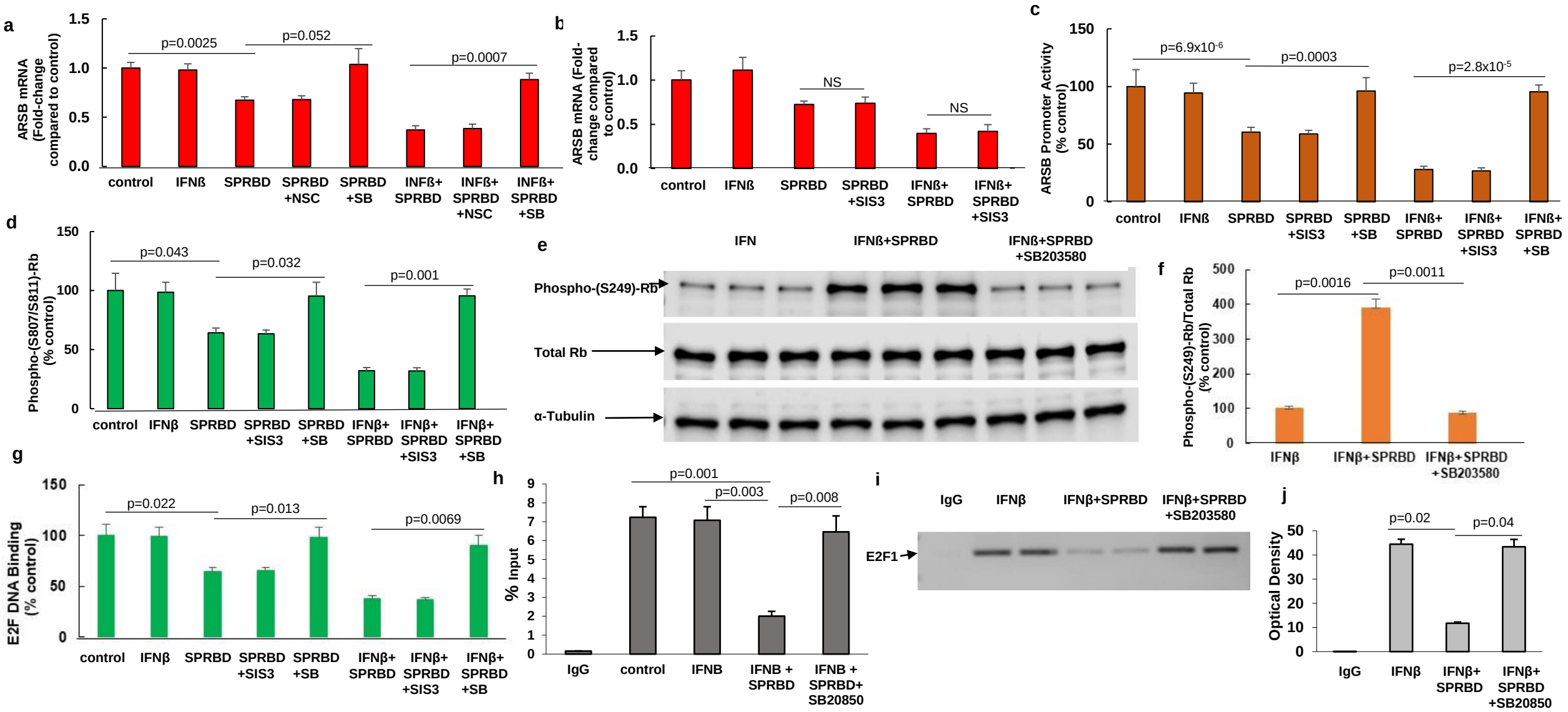

Fig. 4. Effects of desloratadine and monensin on expression of CHST15, CHST11 and ARSB

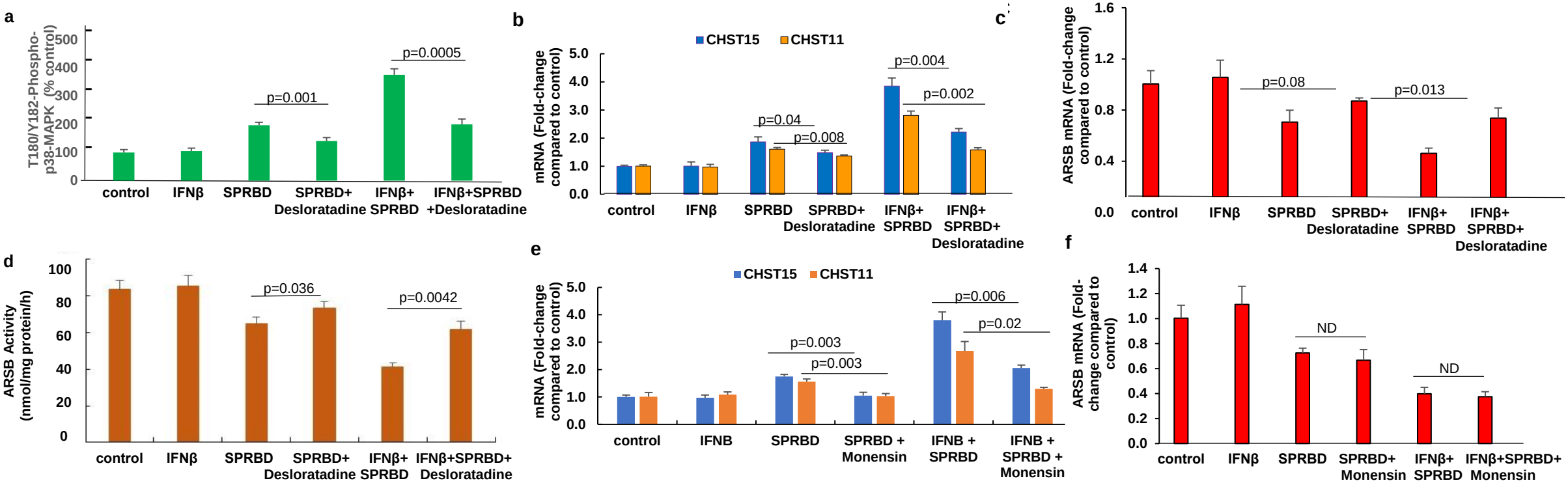
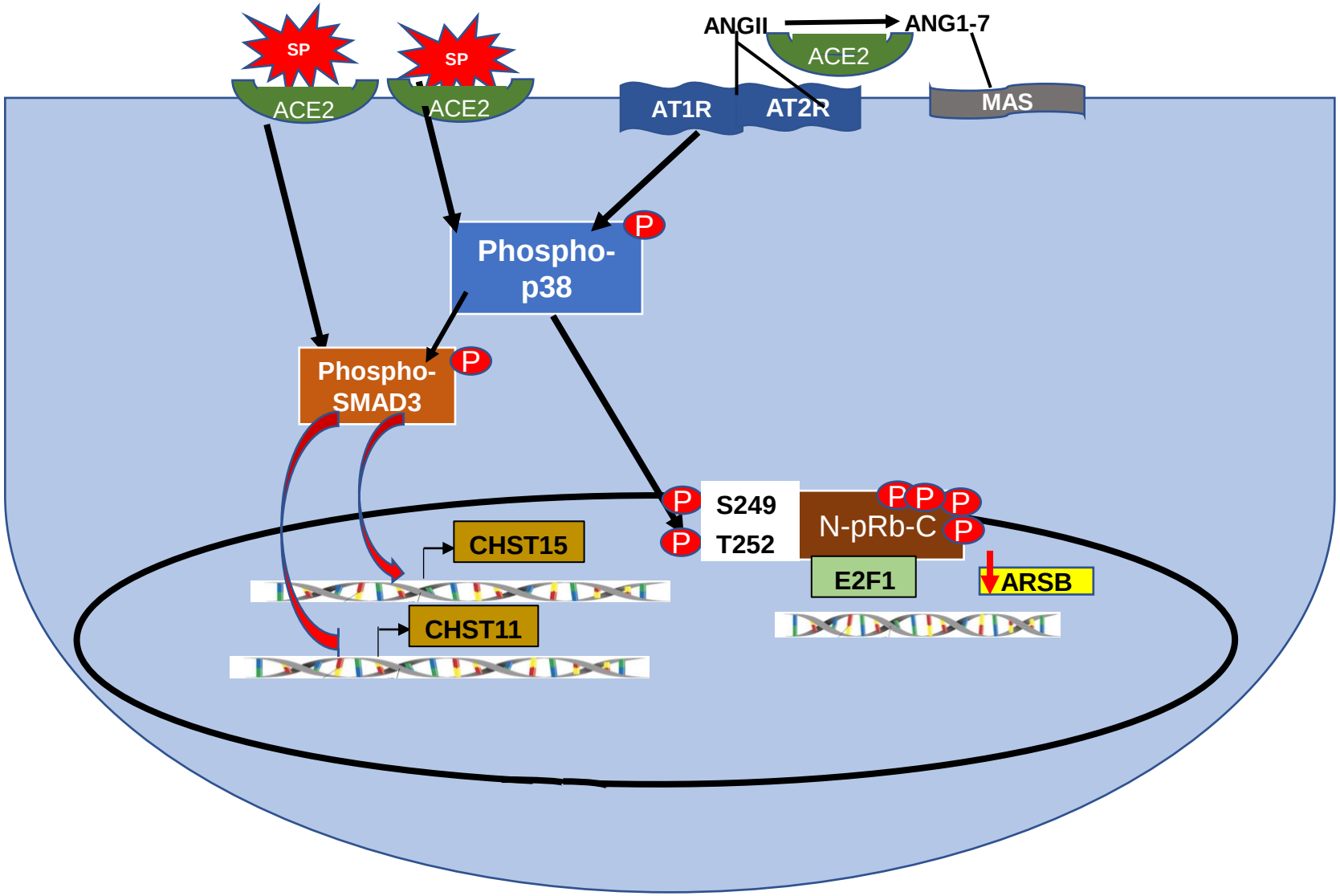
Fig.5. SARS-CoV-2 spike protein binding with ACE2 initiates transcriptional events which modify chondroitin sulfation through activation of phospho-p38 MAPK